NJC

Accepted Manuscript

This is an *Accepted Manuscript*, which has been through the Royal Society of Chemistry peer review process and has been accepted for publication.

Accepted Manuscripts are published online shortly after acceptance, before technical editing, formatting and proof reading. Using this free service, authors can make their results available to the community, in citable form, before we publish the edited article. We will replace this *Accepted Manuscript* with the edited and formatted *Advance Article* as soon as it is available.

You can find more information about *Accepted Manuscripts* in the Information for Authors.

Please note that technical editing may introduce minor changes to the text and/or graphics, which may alter content. The journal's standard Terms & Conditions and the Ethical guidelines still apply. In no event shall the Royal Society of Chemistry be held responsible for any errors or omissions in this *Accepted Manuscript* or any consequences arising from the use of any information it contains.

ROYAL SOCIETY OF CHEMISTRY

www.rsc.org/njc

New Journal of Chemistry

Dynamic Article Links ►

Cite this: DOI: 10.1039/c0xx00000x

www.rsc.org/xxxxxx

Paper

One-step synthesis of Fe_3O_4/carboxylate-rich carbon composite and its application for Cu (□) removal

Lingling Qu,[a,c] Jianzhong Jia,[b] Hefei Shi [b] and Zhijun Luo*[b,c]

Received (in XXX, XXX) Xth XXXXXXXXX 20XX, Accepted Xth XXXXXXXXX 20XX

DOI: 10.1039/b000000x

Fe_3O_4/carboxylate-rich carbon composite (Fe_3O_4/CRC) have been synthesized via a facile one-step low temperature carbonization method from simple precursors, the single iron source $FeSO_4.7H_2O$ and sodium gluconate. Carboxylate groups of sodium gluconate can coordinate with Fe(□) and form the ferricarboxylate complexes. During the low temperature carbonization process, Fe_3O_4 can be obtained through the thermal decomposition of ferricarboxylate complexes. In addition, sodium gluconate can serve as the source of carboxylate functional group of Fe_3O_4/CRC. Due to the lower temperature of carbonization process (300 °C), abundant carboxylate group can be remained in amorphous carbon and serve as the metal-binding functional group to enhance the adsorption affinity between Fe_3O_4/CRC and Cu (□). Fe_3O_4/CRC was found to be an ideal adsorbent for Cu (□) removal with a higher adsorption capacity. We investigated how the contact time, temperature, pH, and initial concentration of Cu (□) can affect the adsorption of Cu (□) on Fe_3O_4/CRC. In addition, we also did some theoretical simulation about the Cu (□) adsorption model. Among the various kinetics models, the pseudo-second-order is the most suitable kinetics model for adsorption of Cu (□) onto Fe_3O_4/CRC. Adsorption of the heavy metals to Fe_3O_4/CRC reached equilibrium in less than 5 min, and agreed well to the Langmuir adsorption model with maximum adsorption capacities 66.67 mg g^{-1} at 25 °C. The adsorption-desorption studies indicated that Fe_3O_4/CRC possesses good stability and good reusability.

1. Introduction

Toxic heavy metal ions such as Cu^{2+}, Cd^{2+}, Hg^{2+}, Cr^{3+} in water bring many detrimental effects on environment and human health. Heavy metal ions could accumulate in living bodies and cause serious diseases even at very low concentration.[1, 2] Therefore, efficient removal of heavy metal ions from water is very important and has attracted considerable research and practical interests. Among these heavy metals, bivalent copper (Cu (Ⅱ)) is a priority pollutant and ingestion of excessive copper may lead to vomiting, cramps, convulsion and even death.[3] Until now, many technologies have been developed to remove Cu (Ⅱ) from effluents, such as chemical precipitation,[4] ion exchange,[5] membrane filtration,[6] electro-coagulation,[7] and adsorption[8]. Among them, Adsorption has been widely used as a simple, economical, and cost-effective technology for the removal of heavy metals from wastewater during the past decade. Adsorbents play a key role in the removal of heavy metal ions since they determine the performance of treatment technology, including adsorption capacity and post-treatment (separation). Various adsorbents have been reported for the removal of Cu (Ⅱ) from aqueous solutions, including zeolites,[9] bentonite,[10] Al_2O_3, [11] chitosan,[12] functionalized polymers, [13] and carbon materials [14].

Carbon materials are the commonly used adsorbents in water treatment systems owing to its large surface area, light weight, low hazard risk and good stability. Many carbon materials, such as activated carbon, carbon nanotubes, graphene, have been investigated for heavy metal removal.[15-17] Good water dispersability and the existence of metal-binding groups on the surface of carbon materials are propitious to the removal of heavy metal ions from water. Unfortunately, the carbonization process of carbon materials usually requires high temperatures (usually pyrolysis above 600 ºC) which induce large numbers of organic functional groups flow away.[18] The lack of functional groups in carbon materials results in poor water dispersability and metal-binding properties. In order to improve the water-solubility and metal-binding properties, the surface of carbon materials must be modified with various agents, such as nitric acid, hydrogen peroxide, ethylenediamine etc..[19-21] These modification processes make the synthesis route of adsorbents more complicated and further expense is required. Compared with the intensive research on activated carbon, carbon nanotubes, graphene, amorphous carbon has been rarely investigated in the heavy metal adsorption applications. The merit of amorphous carbon obtained by hydrothermal carbonization (HTC) process is the rich functional

groups, which can be remained to greatly improve hydrophilicity and chemical reactivity.[22] However, the amount of carboxylic acid groups containing in amorphous carbon obtained by HTC is pretty low, underlining the highly reductive conditions throughout the hydrothermal, oxygen-free carbonization reaction (the constituting aldoses transfer into aldehydes onto the surface), which makes it difficult to obtain the carboxylate-rich carbon materials. [23] In addition, the carbon particle size derived from the HTC process often possess several micrometer and the low surface area of carbon particles limits its application in the heavy metal adsorption. [24,25]

After adsorption process, it is rather difficult to separate and regenerate adsorbents from large volume of environmental samples due to the small particle size of carbon materials. The traditional separation methods, including centrifugation or filtration, are time consuming and high cost. Nanosized Fe_3O_4 particles are considered as potential adsorbents for aqueous heavy metals due to their high surface area and the unique advantage of easy separation under external magnetic fields. However, bare Fe_3O_4 nanoparticles show poor stability under acidic conditions and even are very much susceptible to air oxidation.[26] In addition, nanosized Fe_3O_4 particles are easily aggregated in aqueous systems. To further improve the adsorption affinity, selectivity, and stability, Fe_3O_4 nanoparticles can be modified with an organic compound such as chitosan,[27] humic acid, [28] carboxylated multi-wall carbon nanotube,[29] diethylenetriamine (EDTA)[30]. Obviously, these organic compounds contain rich carboxylate functional group which has potent complex capacity with heavy metal ions. However, these surface modification process need two or several steps and usually was low producing and time consuming, which make the synthesis route complicated and render the adsorbents too expensive for widespread industrial use. [31,32]

The motivation of the present research originated from the idea that the amorphous carbon rich in carboxylate functional group makes it a good candidate for coupling with Fe_3O_4 nanoparticles and improving adsorption performance. Herein, we present a low temperature carbonization process in the air condition for the fabrication of Fe_3O_4/carboxylate-rich carbon composite (Fe_3O_4/CRC). In order to obtain Fe_3O_4/CRC with abundant carboxylate groups, sodium gluconate was introduced for the synthesis of Fe_3O_4/CRC. Via the low temperature carbonization process, abundant carboxylate groups can be remained in amorphous carbon and serve as the metal-binding functional group to enhance the adsorption affinity between adsorbent and Cu (Ⅱ). After completion of the adsorption or desorption, the Fe_3O_4/CRC could be rapidly separated under an applied magnetic field.

2. Experimental Section

2.1. Adsorbent preparation

Preparation of Fe_3O_4/carboxylate-rich carbon composite (Fe_3O_4/CRC)

Fe_3O_4/CRC was synthesized via low temperature carbonization process. $FeSO_4.7H_2O$ (1 g) and sodium gluconate (3 g) were dissolved in 20 mL deionized water and stirred for half an hour. Subsequently, the mixture was evaporated out at 90 ºC and form a gel. Then the gel was heated to 300 ºC and kept at 300 ºC for 3 h in air. After cooling down to room temperature, the black products were collected by vacuum filtration and washed several times with deionized water and absolute ethanol. Finally, the washed precipitation was dried in vacuum oven at 60 ºC for 12 h.

In order to compare with the Fe_3O_4/CRC, CRC (carboxylate-rich carbon) was also synthesized by using sodium gluconate and the synthetic route is the same with Fe_3O_4/CRC. The SEM image and nitrogen adsorption/desorption isotherms were shown in Fig. S2.

Preparation of Fe_3O_4 nanoparticles

$FeCl_3.6H_2O$ (2.43 g) and $FeSO_4.7H_2O$ (1.67 g) were dissolved in 50 mL deionized water under nitrogen gas with vigorous stirring at 80 ºC. Then 2 M NaOH aqueous solutions were added into the solution until the pH of the solution was adjusted to 10. After heating, the black suspension was cooled to room temperature naturally. The black products were collected by vacuum filtration and washed several times with deionized water and ethanol. Finally, the washed precipitate was dried in vacuum oven at 60 ºC for 12 h. The XRD pattern and TEM image were shown in Fig. S3.

2.2. Adsorbent characterization

The phase structure and phase purity of the as-synthesized products were examined by X-ray diffraction (XRD) using a Bruker D8 diffractometer with high-intensity Cu Kα radiation (λ=1.54 Å). The field-emission scanning electron microscope (SEM) measurements were carried out with a Hitachi S-4800 operating at 15 kV. The samples used for SEM were prepared by dispersing of some products in ethanol, then placing a drop of the solution onto the surface of Al column and letting the ethanol evaporate slowly in air. Transmission electron microscopy (TEM) images were taken with a JEOL 2100 transmission electron microscopy operated at 200 kV. Fourier transform infrared (FTIR) spectra of all the samples were measured on a Nicolet Nexus 470. Raman spectra were obtained by using a Renishaw Raman system model 2000 spectrometer. Thermogravimetric (TG) analysis was performed on an integrated thermal analyzer (STA 449C) under a flow of air with a temperature ramp of 5 ºC/min. The BET surface area of the powders was determined from Brunauer-Emmett-Teller (BET) measurements using an ASAP 2020 surface area and porosity analyzer. The Cu (Ⅱ) ions concentrations were measured by Inductive Couple Plasma Mass

Spectrometry (Agilent ICP-MS 7700 series). The zeta potential of Fe_3O_4 nanoparticles and Fe_3O_4/CRC obtained at different pH were measured using a Malvern Zetasizer 2000 potential analyzer.

2.3. Cu (Ⅱ) ions adsorption

Adsorption experiments were carried out in Erlenmeyer flask (250mL), where solution of Cu (Ⅱ) (100 mL) with initial Cu (Ⅱ) ions concentrations range from 2 mg L^{-1} to 10 mg L^{-1} was placed. Before mixing with the adsorbent, the solution of Cu (Ⅱ) was adjusted to a certain pH value using 0.1 M HNO_3 and 0.1 M NaOH. When the desired temperature was reached, about 20 mg of Fe_3O_4/CRC was added into flask. The flask with solution was sealed and shaken in a thermostatic water bath shaker operated at 200 rpm. At the end of the equilibrium period, aqueous sample (5 mL) was taken from the solution, the liquid was separated from the adsorbent magnetically and the concentrations of Cu (Ⅱ) ions were measured using Inductive Couple Plasma Mass Spectrometry (Agilent ICP-MS 7700 series). The amount of Cu (Ⅱ) ions adsorbed at equilibrium, q_e (mg g^{-1}), was calculated by following equation:

$$q_e = \frac{(C_0 - C_e)V}{m} \quad (1)$$

Where C_0 (mg L^{-1}) is the initial concentration of Cu (Ⅱ) ions, C_e (mg L^{-1}) is the equilibrium Cu (Ⅱ) ions concentration in solution, V (L) is the total volume of solution, and m (g) is the adsorbent mass.

The kinetic experiments were identical with those of equilibrium tests. At predetermined moments, aqueous samples (5 mL) were taken from the solution, the liquid was separated from the adsorbent magnetically and concentration of Cu (Ⅱ) ion in solution was determined using Inductive Couple Plasma Mass Spectrometry (Agilent ICP-MS 7700 series)

$$q_t = \frac{(C_0 - C_t)V}{m} \quad (2)$$

Where C_0 (mg L^{-1}) is the initial concentration of Cu (Ⅱ) ions, C_t (mg L^{-1}) is the concentration of Cu (Ⅱ) ion at any time t, V (L) is the total volume of solution, and m (g) is the adsorbent mass.

3. Results and discussion

3.1 Characterization of adsorbents

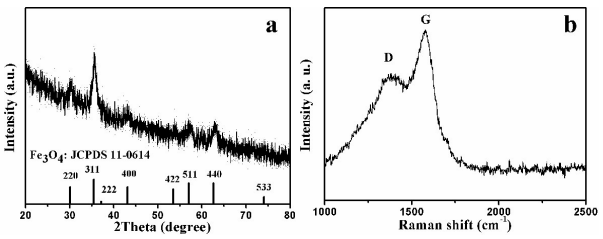

Fig. 1. (a) XRD pattern, and (b) Raman spectra of Fe_3O_4/CRC.

The crystalline and composition of the as-synthesized products were characterized by XRD. The diffraction peaks in Fig. 1a could be indexed as Fd3m cubic Fe_3O_4 (JCPDS card No. 11-0614). No other characteristic peaks such as the impurities of hematite or hydroxides were detected, suggesting high purity of the as-synthesized Fe_3O_4 in Fe_3O_4/CRC by the present low temperature carbonization process. No obvious diffraction peak for the carbon is observed, suggesting the carboxylate-rich carbon is amorphous carbon. The Raman spectra (Fig. 1b) for Fe_3O_4/CRC shows the characteristic wide D and G bands around 1360 and 1580 cm^{-1}, respectively, typical for amorphous carbons. The large I_D/I_G value (0.87) indicates the low degree of graphitization of the carboxylate-rich carbon.

The sizes and morphologies of as-synthesized samples were further investigated by SEM and TEM. Fig. 2a presents the panoramic SEM image of the Fe_3O_4/CRC. SEM image in Fig. 2a shows the Fe_3O_4/CRC are mainly composed of many 2-D sheets and the thickness of these carbon sheets are less than 400 nm (Fig. 2b). Fig. 2c shows the TEM image of verge of Fe_3O_4/CRC. The image clearly indicates that a number of Fe_3O_4 nanoparticles were dispersed into the carbon sheet and the particle size of these Fe_3O_4 nanoparticles is less than 10 nm (Fig. 2d).

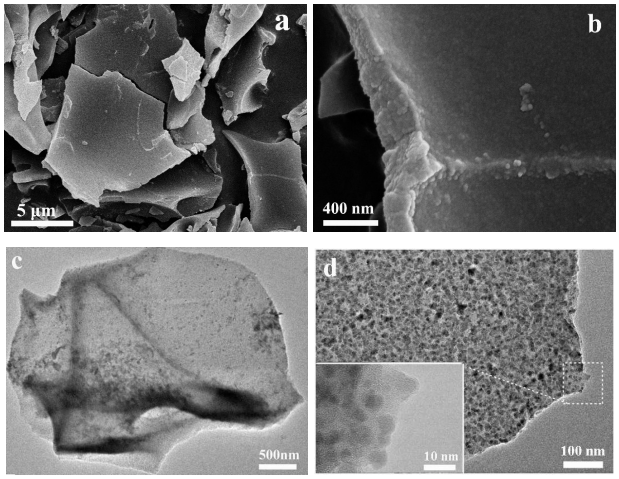

Fig. 2. (a)(b) SEM images, and (c,d) TEM images of Fe_3O_4/CRC

The carbon content is determined by thermogravimetric analysis performed under air (Fig. 3a). It can be noticed that the weight loss below 180 ºC could be probably assigned to the release of the free water and the structural water of Fe_3O_4/CRC. For Fe_3O_4/CRC, the major weight loss take place at 180 ºC and completes at 620 ºC, giving rise to a large weight loss of about 59.29 wt%. While considering that Fe_3O_4 will be converted into Fe_2O_3 when heated in air, the actual carbon content in the Fe_3O_4/CRC can be estimated to be about 46.15%. The FT-IR spectra were further used to investigate the functional groups remained on the surface of Fe_3O_4/CRC. Fig.3b shows the FT-IR spectra curves of Fe_3O_4 nanoparticles and Fe_3O_4/CRC, respectively. The band at 1690 cm^{-1} can be assigned to the

carbonyl in carboxylate group.[23, 25] Two bands located at 1580 and 1400 cm^{-1} can be assigned to the asymmetric and symmetric stretching vibration of COO^- groups, respectively. [33] The band at 580 cm^{-1} is attributed to the Fe-O stretch, which indicates the existence of Fe_3O_4. [34] The bands at 3400 cm^{-1} imply the existence of large numbers of hydroxyl groups. Surface analysis of the Fe_3O_4/CRC was carried out using X-ray photoelectron spectroscopy (XPS). The partial XPS spectra of C1s (Fig. 2c) can be deconvoluted into three component peaks with binding energies at about 284.6, 286.6 and 288.6 eV, which are attributed to the C-C, C-O, and C=O bonds, respectively. The area of C=O component peak makes up about 12.1% of the area of C1s peak, which imply the higher proportions of carboxylate groups in the CRC of Fe_3O_4/CRC. In partial XPS spectra of Fe 2p (Fig. 3d), the peaks for Fe 2p3/2 and Fe 2p1/2 were observed at 711.2 and 724.5 eV, which was also indicative of the formation of a Fe_3O_4 phase in Fe_3O_4/CRC. According to FT-IR and XPS results, it was demonstrated that a large number of carboxylate group and hydroxyl group remained in the Fe_3O_4/CRC. As is well known, carboxylate group is an important functional group which can strongly coordinate with different metal ions and can significantly increase the adsorption of heavy metal ions. [35-37] So, the rich carboxylate groups on the surface of Fe_3O_4/CRC will give an advantage in the application of Cu (Ⅱ) adsorption.

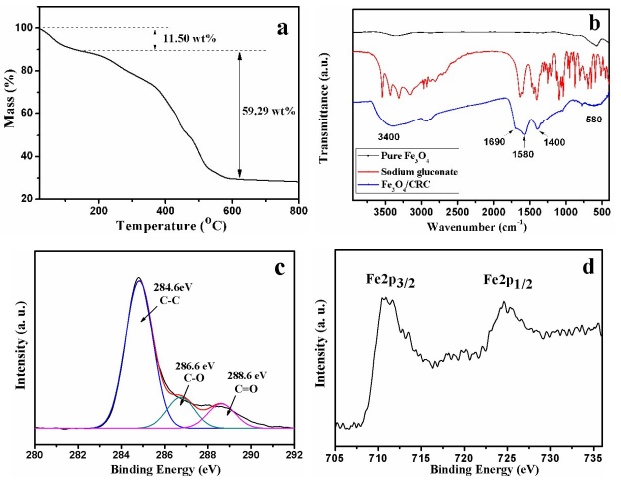

Fig. 3. (a) Thermogravimetric (TG) curve, (b) FT-IR spectra, (c) C 1s XPS spectra, and (d) Fe 2p XPS spectra of Fe_3O_4/CRC.

The surface area, pore volume and pore size distribution of Fe_3O_4/CRC is analyzed by nitrogen adsorption-desorption techniques. As shown in Fig. 4a, it exhibits a type IV isotherm characteristic for mesoporous materials. However, Fe_3O_4/CRC shows narrower hysteresis loop and a steep increase in adsorption at P/P_0 close to 0.9, indicating that it has macropores and broad BJH pore-size distribution(1.8~100 nm), as shown in the Fig. S1. The BET surface area and total pore volume were calculated to be 11.78 m^2g^{-1} and 0.016 cm^3g^{-1}, respectively. Obviously, the low BET surface area of Fe_3O_4/CRC indicates that the adsorption of Cu (Ⅱ) onto Fe_3O_4/CRC should be attributed to chemical adsorption rather than physical adsorption. The zeta potentials of the Fe_3O_4 nanoparticles and Fe_3O_4/CRC were measured at varied pH and presented in Fig. 4b, respectively. The pH of zero point charge (pH_{pzc}) of Fe_3O_4 nanoparticles was 6.1, which is close to the value reported in literature.[31] Due to rich carboxylate group in CRC, the pH_{pzc} of Fe_3O_4/CRC significantly decreased to about 1.4. The zeta potentials of Fe_3O_4/CRC became more negative with increasing suspension pH. Abundant negative charge on their surface of Fe_3O_4/CRC benefits the sorption of positively charged metal ions such as Cu (Ⅱ) ions.

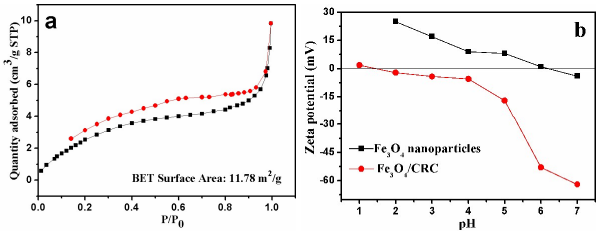

Fig. 4. (a) Nitrogen adsorption/desorption isotherms and pore size distribution (inset), and (b) Zeta potentials of Fe_3O_4/CRC.

Generally, the fabrication of Fe_3O_4/carbon composites requires two steps, the synthesis of Fe_3O_4 and subsequently integrates with carbon, which makes the synthesis route more complicated and renders the adsorbents too expensive for widespread industrial use.[31] During the fabrication process of Fe_3O_4/CRC, different functional groups of sodium gluconate play synergetic roles illustrated in Scheme 1: (1) Sodium gluconate can serve as the source of carboxylate functional group of Fe_3O_4/CRC. Due to the abundant carboxylate group on the surface of Fe_3O_4/CRC, Fe_3O_4/CRC will exhibit excellent adsorption capacity via the complex process between carboxylate group and Cu (Ⅱ). (2) Carboxylate groups of sodium gluconate can complex with Fe (Ⅱ) and form the ferricarboxylate complexes. At low temperature, Fe_3O_4 can be obtained through the thermal decomposition of ferricarboxylate complexes.[38] (3) Sodium gluconate as the derivative of glucose could serve as the carbon source for the CRC. In addition, the stronger binding between carboxylate group and Fe_3O_4 is propitious to the in situ carbon coating on Fe_3O_4 and make the Fe_3O_4 nanoparticles disperse into the CRC.

New Journal of Chemistry

Dynamic Article Links ►

Cite this: DOI: 10.1039/c0xx00000x

www.rsc.org/xxxxxx

Paper

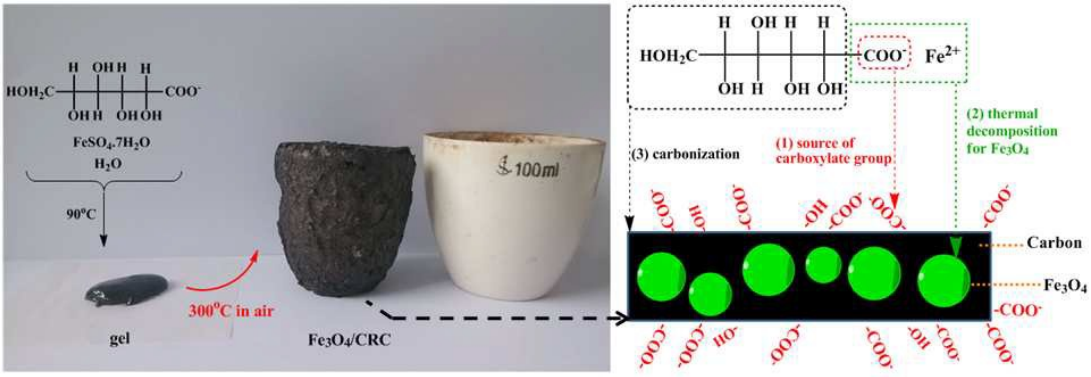

Scheme 1. Functional groups of Sodium gluconate play synergetic roles in the formation of Fe_3O_4/CRC.

3.2 Cu (□) adsorption

3.2.1. Effect of pH

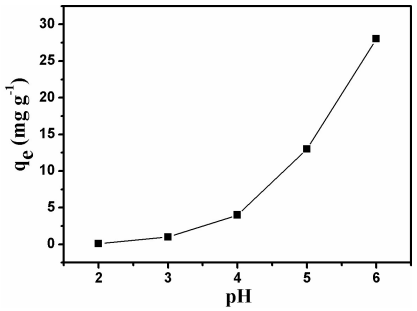

Fig. 5. Effect of pH on the adsorption of Cu (□) by Fe_3O_4/CRC. 25 ºC, initial concentration of Cu (□): 6 mg L^{-1}.

The effect of pH on the adsorption of Cu (□) onto Fe_3O_4/CRC was investigated at pH 2-6, 25 ºC. As illustrated in Fig. 5, the adsorption amount of Cu (□) increases with increasing pH values from 2 to 6 for Fe_3O_4/CRC and almost no Cu (□) is adsorbed at pH=2. The smaller adsorption capabilities of Fe_3O_4/CRC at lower pH levels, are probably due to the significant competition between Cu (□) and hydrogen ions for adsorption sites.[39] As is well known, Cu (Ⅱ) in aqueous solution can present in several forms, such as Cu (□), $Cu(OH)^+$, $Cu(OH)_2$, and $Cu(OH)_4^{2-}$. Cu (□) is the predominant species at pH<6 and the $Cu(OH)_2$ precipitation begin to form when the pH value beyond 6. [40] So, the adsorption of Cu (□) at pH>6 was not investigated and the further experiments were carried out at pH=6.

3.2.2. Adsorption kinetics

It is important to be able to predict the solute uptake rate for the design an sdsorption treatment plant. Kinetics experiments were carried out by adding 20 mg of Fe_3O_4/CRC to 100 mL solution containing various amount of Cu (Ⅱ) at pH 6.0, 25 ºC with contact time ranging from 1 to 60 min. As shown in Fig. 6, the adsorption amount of Cu (Ⅱ) increased with increasing contact time, and the adsorption quickly reaches equilibrium in less than 5 min. the short adsorption equilibrium time implies that the adsorption of Cu (Ⅱ) by Fe_3O_4/CRC takes place in a single step.[41] The adsorption capacity at equilibrium increases evidently from 9.55 to 44.71 mg g^{-1}, with an increase in the initial Cu (Ⅱ) ions concentration from 2 to 10 mg L^{-1}. The result that adsorption capacity of Cu (Ⅱ) increased with the increasing of initial Cu (Ⅱ) concentration might be attributed to an increase in the driving force of concentration gradient with the increase in the initial concentration. In order to investigate the adsorption of Cu (Ⅱ) by using Fe_3O_4 nanoparticles, CRC, and Fe_3O_4/CRC, the adsorption experiments were carried out by adding 20 mg of Fe_3O_4/CRC to 100 mL solution containing 8 mg L^{-1} of Cu (Ⅱ) at pH 6.0, 25 ºC with contact time ranging from 1 to 60 min. Compared to the Fe_3O_4 nanoparticles, CRC and Fe_3O_4/CRC have a shorter adsorption equilibrium time and larger adsorption capacity (Fig. 6b). The adsorption of Cu (Ⅱ) onto CRC, and Fe_3O_4/CRC can quickly reach equilibrium in less than 5 min. However, Fe_3O_4 nanoparticles need 15 min to reach adsorption equilibrium. The adsorption capacity at equilibrium of Fe_3O_4 nanoparticles, CRC and Fe_3O_4/CRC were 9.01, 39.33, and 36.50 mg g^{-1}, respectively. CRC and Fe_3O_4/CRC. It is obvious that the rich carboxylate groups gave Fe_3O_4/CRC and CRC advantage in the application of Cu (Ⅱ) adsorption over the Fe_3O_4 nanoparticles .

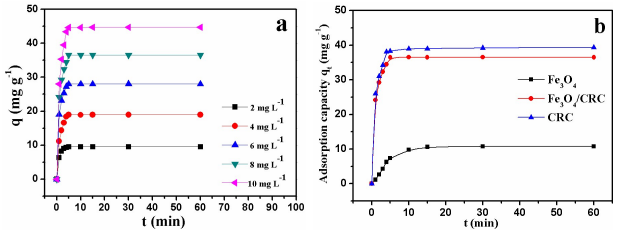

Fig. 6. (a) The kinetic data for Cu (□) uptake by Fe_3O_4/CRC at different initial Cu (Ⅱ) concentration. (b) The adsorption of Cu (Ⅱ) by using Fe_3O_4 nanoparticles, CRC, and Fe_3O_4/CRC. Experimental conditions: C_0=8 mg L^{-1}, pH 6.0.

In order to investigate the adsorption processes of Cu (Ⅱ) on Fe_3O_4/CRC, kinetic analyses were conducted using the Lagergren pseudo-first-order model, the pseudo-second-order model, Elovich model, and intraparticle diffusion model.[30, 31] Lagergren pseudo-first-order model is defined by the following equation:

$$\ln(q_e - q_t) = \ln q_e - k_1 t \quad (3)$$

where q_e and q_t are the sorption capacity (mg g^{-1}) at equilibrium and at time t (min), k is the rate constant, and R^2 is the correlation coefficients from the linear regression to determine the uniformity between the experimental data and model predicted values. The Lagergren pseudo-first-order rate constants k_1 and q_e can be calculated from the slope and intercept of plots of $\ln(q_e-q_t)$ vs. t for different initial concentrations of Cu (Ⅱ). Fig. 7a shows the plot of t/q_t versus t at 25 °C. The calculated k_1, q_e (calc.), and R^2 are presented in Table 1. The correlation coefficients R^2 are in the range of 0.9487-0.9961.

The pseudo-second-order kinetic model is represented by the following linear equation:

$$\frac{t}{q_t} = \frac{1}{k_2 q_e^2} + \frac{1}{q_e} t \quad (4)$$

$$h = k_2 q_e^2 \quad (5)$$

where k_2 (g mg^{-1} min^{-1}) is the rate constant for the pseudo-second-order adsorption kinetics and h (mg g^{-1} min^{-1}) is the initial sorption rate in pseudo-second-order model. Values of k_2 and q_e were calculated from the slope and intercept of the linear plot of t/q_t versus t for different initial concentrations of Cu (Ⅱ) (Fig. 7b). The calculated k_1, q_e (calc.), h, and R^2 are presented in Table 1. The experimental data are in good agreement with the pseudo-second-order model which imply that the rate-limiting step in adsorption is controlled by chemical process. [42]

The Elovich equation is often used to depict the predominantly chemical sorption and can be expressed as

$$q_t = \frac{1}{\beta}\ln(\alpha n(+\frac{1}{\beta}\ln(t) \quad (6)$$

where α is the initial adsorption rate (mg g^{-1} min^{-2}) and β is the desorption constant (g mg^{-1} min^{-1}) related to the extent of surface coverage and activation energy for chemisorption. The value of α and β can be calculated and given in Table 1. As shown in Fig. 7c, the plots of q_t vs. ln(t) show good linear relationship, before reaching the adsorption equilibrium.

Intraparticle diffusion model based on the theory proposed by Weber and Morris is represented by the following equation:

$$q_t = k_3 t^{1/2} + C \quad (7)$$

where C is the intercept and k_3 is the intraparticle diffusion rate constant (g mg^{-1} $min^{-1/2}$). Value of k_3 was obtained from the slope of the linear plot of q_t vs. $t^{1/2}$ (Fig. 7d) and given in Table 1. According to the intraparticle diffusion model proposed by Weber and Morris, if the regression of q_t versus $t^{1/2}$ was linear and passed through the origin, then adsorption process was controlled only by intraparticle diffusion. If the regression was linear, but the plot did not pass through the origin, it suggested that adsorption involved intraparticle diffusion, but that was not the only rate-limiting step.[43] All the intra-particle diffusion rate constants C in this work are not zero which demonstrates that the adsorption process may not be mainly controlled by intraparticle diffusion.

According to mentioned above, it can be concluded that the pseudo-second-order is the most suitable kinetics model for adsorption of Cu (Ⅱ) onto Fe_3O_4/CRC and also suggests that the adsorption process is controlled by chemical adsorption.

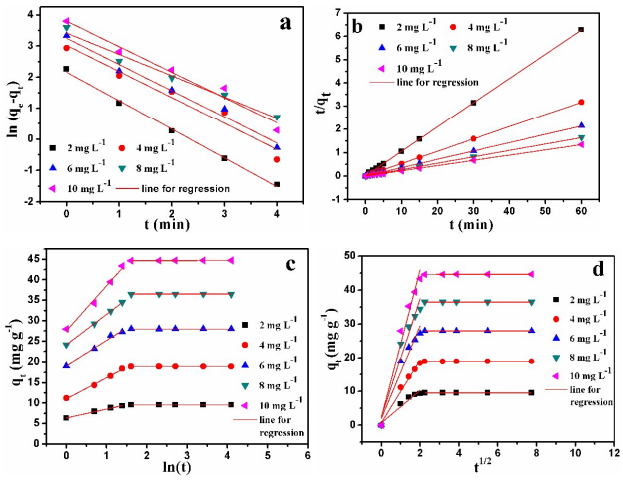

Fig.7. Fitting of Lagergren pseudo-first-order (a), pseudo-second-order (b), Elovich (c), and intraparticle diffusion (d) kinetic models for Cu (□) adsorption on Fe_3O_4/CRC under different initial concentrations (2 mg L^{-1}, 4 mg L^{-1}, 6 mg L^{-1}, 8 mg L^{-1}, and 10 mg L^{-1}) at 25 ºC.

New Journal of Chemistry

Dynamic Article Links ►

Cite this: DOI: 10.1039/c0xx00000x

www.rsc.org/xxxxxx

Paper

Table 1
Kinetic parameters of various models fitted to experimental

Kinetic models and parameters	Cu (□) C_0 (mg L^{-1})				
	2	4	6	8	10
q_e (exp.) (mg g^{-1})	9.55	18.96	28.01	36.50	44.71
Lagergren pseudo-first order equation					
q_e (calc.) (mg g^{-1})	8.67	20.49	25.80	30.49	44.66
k_1 (min^{-1})	0.9195	0.8376	0.8441	0.6859	0.8200
R^2	0.9961	0.9487	0.9750	0.9752	0.9646
Pseudo-second-order equation					
q_e (calc.) (mg g^{-1})	9.58	19.08	28.14	36.70	44.96
k_2 (g mg^{-1} min^{-1})	0.6576	0.1933	0.1846	0.1254	0.0904
h (mg g^{-1} min^{-1})	60.35	70.37	146.20	168.92	182.82
R^2	0.9999	0.9998	0.9998	0.9999	0.9997
Elovich equation					
q_e (calc.) (mg g^{-1})	9.71	19.17	27.67	36.21	44.97
α (mg g^{-1} min^{-2})	48.35	45.88	159.92	164.37	140.61
β (g mg^{-1} min^{-1})	0.4918	0.1993	0.1795	0.1287	0.0929
R^2	0.9862	0.9917	0.9726	0.9864	0.9898
Intra-particle diffusion equation					
q_e (calc.) (mg g^{-1})	10.69	20.47	30.79	39.61	44.99
k_3 (g mg^{-1} $min^{-1/2}$)	4.33	8.63	12.55	16.1586	20.1612
C	1.0221	1.1997	2.9306	3.5448	3.6382
R^2	0.9065	0.9663	0.9165	0.9271	0.9473

3.2.3. Adsorption isotherms

The analysis of the isotherm data by seeing how well different models can accommodate them is an important step in establishing a model that can be successfully used for design purposes. In this study, Langmuir and Freundlich isotherms were used to describe the equilibrium adsorption. [37,41] The Langmuir isotherm model is expressed as the following linear equation:

$$\frac{C_e}{q_e} = \frac{C_e}{q_m} + \frac{1}{q_m K_L} \quad (8)$$

where Ce is the equilibrium concentration of Cu (□) (mg L^{-1}), q_e is the amount of Cu (□) adsorbed on the adsorbent at equilibrium(mg g^{-1}), q_m is the maximum adsorption capacity, and K_L is the Langmuir adsorption constant (L mg^{-1}). The values of q_m and K_L can be calculated from the slope and intercept of linear plots C_e/q_e vs. C_e (figure not shown), and the fitting results are shown in Table 2.

Table 3 compares the maximum adsorption capacity of Fe_3O_4/CRC with different adsorbents based on Fe_3O_4 previously used for removal of Cu (□) from aqueous solutions at 25 ºC. As seen, the maximum adsorption capacity Cu (□) onto Fe_3O_4/CRC is higher than that many other previously reported adsorbents.

The essential characteristics of the Langmuir isotherm can be expressed in terms of a dimensionless equilibrium parameter R_L, which is defined by the following equation:

$$R_L = \frac{1}{1 + K_L C_0} \quad (9)$$

The parameter R_L indicates the type of the isotherm accordingly: R_L>1, unfavorable; R_L=1, liear; 0< R_L<1, favorable and R_L=0, irreversible. In our case, the value of R_L was found to be 0.081 and suggested that the Fe_3O_4/CRC is favorable for Cu (□) adsorption under the conditions mentioned.

The Freundlich isotherm gives a description of equilibrium on heterogeneous surfaces and hence does not assume monolayer capacity. The isotherm is given by the following equation:

$$\ln q_e = \ln K_F + \frac{1}{n} \ln C_e \quad (10)$$

Where K_F and n are the Frendlich constants, n giving an indication of how favorable the adsorption process and K_F [mg g^{-1}(L $mg^{-1})^{1/n}$]. The values of K_F and n can be obtained from the slope and intercept of the linear plots of ln(q_e) vs. ln(C_e), respectively. The value of n is 1.61 at 25 ºC and lie in the range of 1-10, which reveals that adsorption is favorable, which are confirmed with the result of Langmuir model.

Cite this: DOI: 10.1039/c0xx00000x

www.rsc.org/xxxxxx

Paper

Table 2
Langmuir and Freundlich parameters for the adsorption of Cu (Ⅱ) onto Fe_3O_4/CRC at 25 ºC.

T (ºC)	Langmuir isotherm				Freundlich isotherm		
	q_m (mg g^{-1})	K_L (L/mg)	R_L	R^2	n	K_F [mg g^{-1}(Lmg^{-1})$^{1/n}$]	R^2
25	66.67	1.88	0.081	0.9953	1.61	46.06	0.9782

Table 3
Comparison of adsorption capacity of various adsorbents based on Fe_3O_4 for Cu (Ⅱ)

Adsorbents	Capacity (mg g^{-1})	Refs.
Humic acid coated Fe_3O_4 nanoparticles	46.3	28
EDTA functionalized Fe_3O_4 nanoparticles	46.27	30
Amino-functionalized Fe_3O_4@SiO_2 nanomaterials	30.08	31
Chitosan-bound Fe_3O_4 nanoparticles	21.5	32
3-aminopropyltriethoxysilane (APTES) and glutaraldehyde (GA) modified Fe_3O_4 nanoparticles	61.07	41
Fe_3O_4 nanoparticles	8.9	44
Chitosan/clay/ Fe_3O_4 composite	14.3	45
Fe_3O_4/CRC	66.67	This work

3.2.4. Thermodynamic analyses

The thermodynamic parameters provide in-depth information regarding the inherent energetic changes connected with adsorption. Gibbs free energy (ΔG^o), enthalpy (ΔH^o) and entropy (ΔS^o) were calculated as following equation:

$$\Delta G^0 = -RT\ln K \quad (11)$$

$$K = \frac{q_e}{C_e} \quad (12)$$

$$\ln K = -\frac{\Delta H^0}{RT} + \frac{\Delta S^0}{R} \quad (13)$$

where T is the absolute temperature (K), R is the gas constant (8.3145 J mol^{-1} K^{-1}). The effects of temperature on adsorption were investigated at pH 6.0, 298-328K, and the initial Cu (Ⅱ) ion concentration of 6 mg L^{-1}. ΔH^o and ΔS^o were calculated from the slope and intercept from the plot of ln q_e/C_e vs. 1/T (Fig. 8). The results are shown in Table 4. The positive value of ΔH^o (34.74 kJ mol^{-1}) indicate that adsorption of Cu (Ⅱ) onto Fe_3O_4/CRC is an endothermic process. The positive value ΔS^o (151.90 J mol^{-1} K^{-1}) suggests that the randomness increased at the solid-liquid interface during the adsorption of Cu (Ⅱ) onto Fe_3O_4/CRC. The negative value ΔG^o (151.90 kJ mol^{-1}) confirms that the adsorption is spontaneous. When the temperature increases from 298 to 328 K, ΔG^o changes from -10.53 to -15.16 kJ mol^{-1}, suggesting that adsorption is more spontaneous at higher temperature.

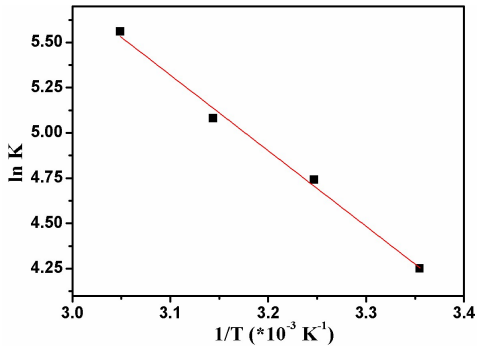

Fig.8. Effect of temperature on the adsorption of Cu (Ⅱ) onto Fe_3O_4/CRC

Table 4
Thermodynamic parameters for the adsorption of Cu (Ⅱ) onto Fe_3O_4/CRC

Cu (Ⅱ) concentration	ΔH^o	ΔS^o	ΔG^o at temperature (K) (kJ mol^{-1})			
(mg L^{-1})	(kJ mol^{-1})	(J mol^{-1} K^{-1})	298	308	318	328
6	34.74	151.90	-10.53	-12.14	-13.43	-15.16

New Journal of Chemistry

Dynamic Article Links ►

Cite this: DOI: 10.1039/c0xx00000x

www.rsc.org/xxxxxx

Paper

3.2.5. Magnetic properties and regeneration

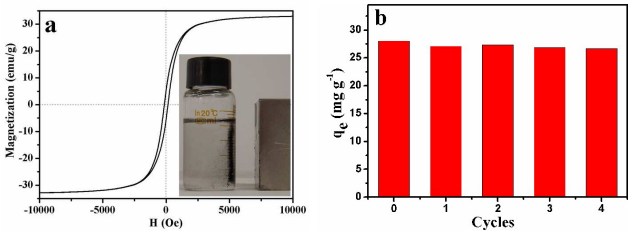

Fig.9. (a) Field-dependent magnetization curve of Fe_3O_4/CRC at room temperature, inset shows the strong attraction of the particles suspended in water toward a magnet; (b) Cu (Ⅱ) adsorption on Fe_3O_4/CRC with four adsorption-regeneration cycles at 25 ºC (initial Cu (Ⅱ) concentration, 6 mg L^{-1})

After the adsorption, the Fe_3O_4/CRC could be rapidly separated under an applied magnetic field. As shown, the Fe_3O_4/CRC is strongly attracted to a permanent magnet (inset in Fig. 9a). The magnetic properties of Fe_3O_4/CRC were studied by using a superconducting quantum interference device (SQUID) magnetometer at room temperature. Fig. 9a display hysteresis loop of Fe_3O_4/CRC, which indicates that it possesses magnetic saturation (Ms) values of about 33 emu g^{-1}.

The regeneration of adsorbent is a crucial factor in practical application of the adsorbent. According to the result of adsorption of Cu (Ⅱ) ions at different pH value (Fig. 5), the suppressed adsorption of Cu (Ⅱ) ions observed on Fe_3O_4/CRC at low pH implies that acid treatment is a feasible approach to regenerating the adsorbent. After the adsorption in initial concentration of 6 mg L^{-1}, the Cu (Ⅱ) loaded Fe_3O_4/CRC are resuspended in 0.01 M HNO_3 solution with sonication 2 min to desorb the Cu (Ⅱ) from Fe_3O_4/CRC. After the suspension was magnetically separated, the concentration of Fe in this HNO_3 solution was determined by ICP-MS. It is found that the percentage of residual Fe is 0.0135 % compared to the amount of Fe in the used Fe_3O_4/CRC which implies that the percent recovery of the Fe_3O_4/CRC is 99.98%. The regenerated Fe_3O_4/CRC was reused in adsorption in four consecutive cycles. Adsorption efficiency of the regenerated adsorbents was shown in Fig. 9b, from which we can see that the adsorption capacity decreases slightly after each cycle. These results indicate that Fe_3O_4/CRC possess good reusability and stability.

4. Conclusion

A simple low temperature carbonization method in the air was used to fabricate Fe_3O_4/CRC. The method is highly sustainable, using $FeSO_4.7H_2O$ as single iron source and sodium gluconate derived from the fermentation of glucose as the source of carboxylate functional group and carbon source. Due to the lower temperature of carbonization process, abundant carboxylate group can be remained in amorphous carbon and serve as the metal-binding functional group to enhance the adsorption affinity between adsorbent and Cu (Ⅱ). The studies showed that Fe_3O_4/CRC had high adsorption capacity for Cu (Ⅱ) and could reach the adsorption equilibrium in less than 5 min. Among the various kinetics and isotherm models, the pseudo-second-order model and the Langmuir model are the most suitable kinetics model and isotherm model for adsorption of Cu (Ⅱ) onto Fe_3O_4/CRC, respectively. The adsorption process was spontaneous and endothermic. Due to the carbon coating on the Fe_3O_4, Fe_3O_4/CRC exhibits good stability in acidic condition. The metal loaded Fe_3O_4/CRC could be recovered readily from aqueous solution by magnetic separation and regenerated easily by acid treatment.

Acknowledgments

We thank Dr. Xiazhang Li in Changzhou University for his help with TEM characterization. This work was financially supported by the Natural Science Foundation of Jiangsu Province (BK20130485), Universities Natural Science Foundation of Jiangsu Province (12KJD150003), Highly Qualified Professional Initial Funding of Jiangsu University (12JDG052), and Jiangsu Collaborative Innovation Center of Technology and Material of Water Treatment.

Notes and references

[a] *School of Chemistry and Chemical Engineering, Jiangsu University, Zhenjiang, 212013, P. R. China*

[b] *School of The Environment, Jiangsu University, Zhenjiang, 212013 P. R. China; E-mail: lzj@ujs.edu.cn*

c State Key Laboratory of Coordination Chemistry, Nanjing University, Nanjing 210093, P. R. China

References

1 K. Kawata, H. Yokoo, R. Shimazaki, S. Okabe, Classification of heavy-metal toxicity by human DNA microarray analysis, *Environ. Sci. Technol.*, 2007, **41**, 3769-3774.

2 I. V. N. Rathnayake, M. Megharaj, G. S. Krishnamurti, N. S. Bolan, R. Naidu, Heavy metal toxicity to bacteria - Are the existing growth media accurate enough to determine heavy metal toxicity?, *Chemosphere,* 2013,

90, 1195-1200.

3 C. Lin, Y. Wu, W. Lu, A. Chen, and Y. Liu, Water chemistry and ecotoxicity of an acid mine drainage-effected stream in subtropical China during a major flood event, *J. Hazard. Mater*., 2007, **142**, 199-207.

4 C. I. Lee, W. F. Yang, C. I. Hsieh, Removal of Cu(II) from aqueous solution in a fluidized-bed reactor, *Chemosphere*, 2004, **57**, 1173-1180.

5 A. Carreon-Alvarez, A. Herrera-Gonzalez, N. Casillas, R. Prado-Ramirez, M. Estarron-Espinosa, V. Soto, W. de la Cruz, M. Barcena-Soto, S. Gomez-Salazar, Cu (II) removal from tequila using an ion-exchange resin, *Food Chem.*, 2011, **127**, 1503-1509.

6 V. Florse, C. Cabassud, A hybrid membrane process for Cu(II) removal from industrial wastewater comparison with a conventional process system, *desalination*, 1999, **126**, 101-108

7 I. Heidmann, W. Calmano, Removal of Ni, Cu and Cr from a galvanic wastewater in an electrocoagulation system with Fe- and Al-electrodes, *Sep. Purif. Technol.*, 2010, **71**, 308-314.

8 A. Q. Dong, J. Xie, W. M. Wang, L. P. Yu, Q. Liu, Y. P. Yin, A novel method for amino starch preparation and its adsorption for Cu(II) and Cr(VI), *J. Hazard. Mater*., 2010, **181**, 448-454.

9 S. b. Wang, T. Terdkiatburana, M. O. Tade, Adsorption of Cu(II), Pb(II) and humic acid on natural zeolite tuff in single and binary systems, *Sep. Purif. Technol*., 2008, **62**, 64-70.

10 E. Eren, B. Afsin, An investigation of Cu(II) adsorption by raw and acid-activated bentonite: A combined potentiometric, thermodynamic, XRD, IR, DTA study, *J. Hazard. Mater*., 2008, **151**, 682-691.

11 W. l. Sun, K. Yin, X. Q. Yu, Effect of natural aquatic colloids on Cu(II) and Pb(II) adsorption by Al_2O_3 nanoparticles, Chem. Eng. J., 2013, **225**, 464-473.

12 D. G. Liu, Z. H. Li, Y. Zhu, Z. X. Li, R. Kumar, Recycled chitosan nanofibril as an effective Cu(II), Pb(II) and Cd(II) ionic chelating agent: Adsorption and desorption performance, *Carbohyd. Polym*. 2014, **111**, 469-476.

13 H. Y. Shen, S. D. Pan, Y. Zhang, X. L. Huang, H. X. Gong, A new insight on the adsorption mechanism of amino-functionalized nano-Fe_3O_4 magnetic polymers in Cu(II), Cr(VI) co-existing water system, *Chem. Eng. J.,* 2012, **183**, 180-191.

14 F. M. Pellera, A. Giannis, D. Kalderis, K. Anastasiadou, R. Stegmann, J. Y. Wang, E. Gidarakos, Adsorption of Cu(II) ions from aqueous solutions on biochars prepared from agricultural by-products, *J. Environ. Manage.*, 2012, **96**, 35-42.

15 M. A. A. Zaini, Y. Amano, M. Machida, Adsorption of heavy metals onto activated carbons derived from polyacrylonitrile fiber, *J. Hazard. Mater*., 2010, **180**, 552-560.

16 S. Rosenzweig, G. A. Sorial, E. Sahle-Demessie, D. C. McAvoy, Optimizing the physical-chemical properties of carbon nanotubes (CNT) and graphene nanoplatelets (GNP) on Cu(II) adsorption, *J. Hazard. Mater.*, 2014, **279**, 410-417.

17 A. Stafiej, K. Pyrzynska, Adsorption of heavy metal ions with carbon nanotubes, *Sep. Purif. Technol*., 2007, **58**, 49-52.

18 I. V. Anoshkin, A. G. Nasibulin, Y. Tian, B. Liu, H. Jiang, E. I. Kauppinen, Hybrid carbon source for single-walled carbon nanotube synthesis by aerosol CVD method, *Carbon*, 2014, **78**, 130-136.

19 Y. Li, H. Li, A. Petz, S. K. Máté, Reducing structural defects and improving homogeneity of nitric acid treated multi-walled carbon nanotubes, *Carbon*, 2015, **93**, 515-522.

20 M. Filkusová, A. Fedorková, R. Oriňáková, A. Oriňák, Z. Nováková, L. škantárová, Modification of carbon nanotubes with sodium p-aminobenzenesulfonate and its effect on Cu^{2+} adsorption, *Carbon*, 2013, **56**, 392-395.

21 M. Hadavifar, N. Bahramifar, H. Younesi, Q. Li, Adsorption of mercury ions from synthetic and real wastewater aqueous solution by functionalized multi-walled carbon nanotube with both amino and thiolated groups, *Chem. Eng. J*., 2014, **237**, 217-228.

22 B. Hu, S. H. Yu, K. Wang, L. Liu, X. W. Xu, Functional carbonaceous materials from hydrothermal carbonization of biomass: an effective chemical process, *Dalton Trans.*, 2008, **40**, 5389-5512.

23 R. D. Cakan, N. Baccile, M. Autonietti, M. M. Titirici,Carboxylate-rich carbonaceous materials via one-step hydrothermal carbonization of glucose in the presence of acrylic acid, *Chem. Mater.*, 2009, **21**, 484-490

24 B. B. Hu, K. Wang, L. H. Wu, S. H. Yu, M. Autonietti, M. M. Titirici,Engineering carbon materials from the hydrothermal carbonization process of biomass, *Adv. Mater.*, 2010, **22**, 813-828.

25 Z. J. Luo, H. J. Tang, L. L. Qu, T. T. Han, X. Y. Wu, A visible-light-driven solid state photo-Fenton reagent based on magnetite-carboxylate-rich carbon spheres, *CrystEngComm*, 2012, **14**, 5710-5713,

26 D. Maity, D. C. Agrawal, Synthesis of iron oxide nanoparticles under oxidizing environment and their stabilization in aqueous and non-aqueous media, *J. Magn. Magn. Mater.*, 2007, **308**, 46-55.

27 Z. Liu, H. S. Wang, C. Liu, Y. J. Jiang, G. Yu, X. D. Mu, X. Y. Wang, Magnetic cellulose-chitosan hydrogels prepared from ionic liquids as reusable adsorbent for removal of heavy metal ions, *ChemComm,* 2012, **48**, 7350-7352.

28 J. F. Liu, Z. S. Zhao, G. B. Jiang, Coating Fe_3O_4 magnetic nanoparticles with humic acid for high efficient removal of heavy metals in water, Environ. Sci. Technol., 2008, 42, 6949-6954.

29 D. L. Xiao, H. Li, H. He, R. Lin, P. L. Zuo, Adsorption performance of carboxylated multi-wall carbon nanotube-Fe_3O_4 magnetic hybrids for Cu(II) in water, *New Carbon Mate.*, 2014, **29**,15-25.

30 Y. Liu, M. Chen, Y. M. Hao, Study on the adsorption of Cu(II) by EDTA functionalized Fe_3O_4 magnetic nano-particles, *Chem. Eng. J*., 2013, **218**, 46-54.

31 J. H. Wang, S. R. Zheng, Y. Shao, J. L. Liu, Z. Y. Xu, D. Q. Zhu, amino-functionalized Fe_3O_4@SiO_2 core–shell magnetic nanomaterial as a novel adsorbent for aqueous heavy metals removal, *J. Colloid Interf. Sci*., 2010, **349**, 293-299.

32 Y. C. Chang, D. H. Chen, Preparation and adsorption properties of monodisperse chitosan-bound Fe_3O_4 magnetic nanoparticles for removal of Cu(II) Ions, *J. Colloid Interf. Sci.*, 2005, **283**, 446-451.

33 X. J. Tong, J. Y. Li, J. H. Yuan, R. K. Xu, Adsorption of Cu(II) by biochars generated from three crop straws, *Chem. Eng. J.*, 2011, **172**, 828-834.

34 F. Y. Cao, C. L. Chen, Q. Wang, Q. W. Chen, Synthesis of carbon–Fe_3O_4 coaxial nanofibres by pyrolysis of ferrocene in supercritical carbon dioxide, *Carbon*, 2007, **45**, 727-731.

35 C. K. Liu, R. B. Bai, Extended study of deta-functionalized pgma adsorbent in the selective adsorption behaviors and mechanisms for heavy metal ions of Cu, Co, Ni, Zn, and Cd, *J. Colloid Interf. Sci.*, 2010, **350**, 282-289.

36 E. Repo, J. K. Warchol, A. Bhatnagar, A. Mudhoo, M. Sillanpaa, Aminopoly -carboxylic acid functionalized adsorbents for heavy metals removal from water, *Water Res.*, 2013, **47**, 4812-4832.

37 D. Kolodyńska, Z. Hubicki, M. Geca, Polyaspartic acid as a new complexing agent in removal of heavy metal ions on polystyrene anion exchangers, *Ind. Eng. Chem. Res.*, 2008, **47**, 6221-6227.

38 M. Hermanek, R. Zboril, M. Mashlan, L. Machala, O. Schneeweiss, Thermal behavior of iron (Ⅱ) oxalate dehydrate in the atmosphere of its conversion gases, *J. Mater. Chem.*, 2006, **16**, 1273-1280.

39 S. S. Banerjee, D. H. Chen, Fast removal of copper ions by gum arabic modified magnetic nano-adsorbent, *J. Hazard. Mater.*, 2007, **147**, 792-799.

40 G. D. Sheng, J. X. Li, D. D. Shao, J. Hu, C. L. Chen, Y. X. Chen, X. K. Wang, Adsorption of copper(II) on multiwalled carbon nanotubes in the absence and presence of humic or fulvic acids, *J. Hazard. Mater.*, 2010, **178**, 333-340.

41 M. Ozmen, K. Can, G. Arslan, A. Tor, Y. Cengeloglu, M. Ersoz, Adsorption of Cu(II) from aqueous solution by using modified Fe_3O_4 Magnetic Nanoparticles, *Desalination*, 2010, **254**, 162-169.

42 Y. F. Lin, H. W. Chen, P. S. Chien, C. S. Chiou, C. C. Liu, Application of bifunctional magnetic adsorbent to adsorb metal cations and anionic dyes in aqueous solution, *J. Hazard. Mater.*, 2011, **185**, 1124-1130.

43 R. R. Sheha, A. A. El-Zahhar, Synthesis of some ferromagnetic composite resins and their metal removal characteristics in aqueous solutions, *J. Hazard. Mater.*, 2008, **150**, 795-803.

44 X. S. Wang, L. Zhu, H. J. Lu, Surface chemical properties and adsorption of Cu (II) on nanoscale magnetite in aqueous solutions, *Desalination*, 2011, **276**, 154-160.

45 D. W. Cho, B. H. Jeon, C. M. Chon, Y. J. Kim, F. W. Schwartz, E. S. Lee, H. Song, A novel chitosan/clay/magnetite composite for adsorption of Cu(II) and As(V), *Chem. Eng. J.*, 2012, **200-202**, 654-662.

Graphical Abstract:

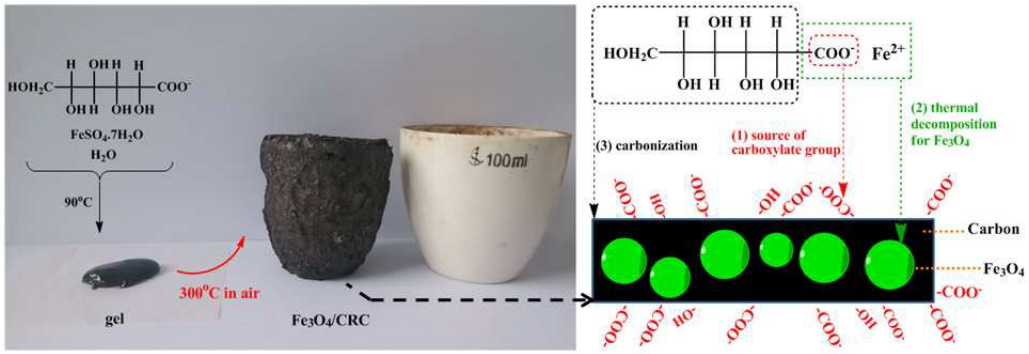

A magnetically separable adsorbent, Fe_3O_4/carboxylate-rich carbon composite was synthesized via a facile one-step low temperature carbonization process.